Optimal control of ultrafast laser driven many-electron dynamics in a polyatomic molecule: N-methyl-6-quinolone

Tillmann Klamroth

Citation: J. Chem. Phys. **124**, 144310 (2006); doi: 10.1063/1.2185633
View online: http://dx.doi.org/10.1063/1.2185633
View Table of Contents: http://jcp.aip.org/resource/1/JCPSA6/v124/i14
Published by the American Institute of Physics.

Optimal control of ultrafast laser driven many-electron dynamics in a polyatomic molecule: *N*-methyl-6-quinolone

Tillmann Klamroth[a)]
Theoretische Chemie, Institut für Chemie, Universität Potsdam, Karl-Liebknecht-Straße 24-25, D-14476 Golm, Germany

(Received 25 October 2005; accepted 15 February 2006; published online 13 April 2006)

We report time-dependent configuration interaction singles calculations for the ultrafast laser driven many-electron dynamics in a polyatomic molecule, *N*-methyl-6-quinolone. We employ optimal control theory to achieve a nearly state-selective excitation from the S_0 to the S_1 state, on a time scale of a few ($\approx$6) femtoseconds. The optimal control scheme is shown to correct for effects opposing a state-selective transition, such as multiphoton transitions and other, nonlinear phenomena, which are induced by the ultrashort and intense laser fields. In contrast, simple two-level π pulses are not effective in state-selective excitations when very short pulses are used. Also, the dependence of multiphoton and nonlinear effects on the number of states included in the dynamical simulations is investigated. © *2006 American Institute of Physics*.
[DOI: 10.1063/1.2185633]

I. INTRODUCTION

The real time monitoring and control of elementary reaction steps in molecular systems by ultrashort laser pulses has attracted much attention recently.[1] While early experimental and theoretical applications were mainly concerned with the nuclear dynamics (see, for example, Ref. 2 and references therein), more recent pump-probe laser experiments[3] have shown that one can follow also the electron dynamics with a subfemtosecond resolution. This subfemtosecond or attosecond time scale is the natural time scale for the dynamical rearrangement of the electrons.[4,5] Because of the impressive advances in laser technology, e.g., the possibility to measure the phase between the carrier and the pulse envelope of a few cycle laser pulse,[6,7] it should also be possible to control selectively the electronic state of a molecule with ultrashort laser pulses on a time scale of a few femtoseconds, where nuclear motion can usually be neglected. However, such a selective control is a nontrivial task, because due to the large spectral width and the typically high intensity of ultrashort laser pulses, not a state-selective excitation occurs but a coherent superposition of excited states is created instead. Further, multiphoton transitions and other effects governed by the polarizability or higher order polarizabilities might become dominant.[8]

In this paper we report explicitly time-dependent simulations of the laser driven many-electron dynamics in a polyatomic molecule, *N*-methyl-6-quinolone, and combine it with optimal control theory (OCT).[9,10] Here, we explore the possibility to induce a state-selective excitation of the molecule from the S_0 to the S_1 state within a time interval as short as 6 fs. The practical interest in this molecule arises from the observation that it can be used as a probe for the ultrafast solvation dynamics in condensed phase,[11] because the geometrical change of the molecule in the excited state is very small but at the same time a large change in the permanent dipole moment occurs. It has been shown that the underlying model for many-electron dynamics used here, i.e., a time-dependent configuration interaction method,[12] is capable to account at least to some extent for the nonlinear effects induced by ultrashort and intense laser pulses.[8] In this paper we present the results which indicate that despite the strong nonlinear effects it is still possible to achieve a nearly state-selective ultrafast excitation in *N*-methyl-6-quinolone, at least in our model calculations, by means of the OCT.

This paper also serves the purpose to extend explicitly time-dependent electron dynamics to larger systems. Many-electron dynamics is a challenging subject and much effort has been put into the development of suitable methods. An exact solution of the time-dependent Schrödinger equation is presently possible only for molecules such as H_2 (Ref. 13) or simple atoms such as Be,[14] i.e., for few electron systems. Nevertheless, the well established methodology in electronic structure theory offers a wide range of methods which can be adapted for explicitly time-dependent problems. The earliest developments are probably the time-dependent Hartree-Fock[15] (TD-HF) and the (explicitly) time-dependent density functional theory (TD-DFT).[16] Both methods use a single Slater determinant to represent the electronic wave function or the density, respectively. In TD-HF electron correlation is neglected, while TD-DFT treats dynamical electron correlation via an exchange correlation functional. Another way to account for the electron correlation is to use a multideterminant description. For example, a time-dependent variant of the complete active space self-consistent field (CASSCF) method[17] was proposed,[18–20] which accounts both for dynamical and static correlations. In this paper we will use the time-dependent configuration interaction (TD-CI) method with singles (TD-CIS) excitations.[12] This method accounts for some electron correlation at least in the excited

[a)]Electronic mail: klamroth@rz.uni-potsd

states, and has been used recently[8] for laser driven, ultrafast electron dynamics in a small molecule, LiCN.

In this paper we use the phrase TD in TD-CIS to indicate that we treat the electron dynamics explicitly time dependent within an *ab initio* wave function approach and the fixed nuclei approximation, and not the time dependence of both the electrons and the nuclei as, for example, done in Refs. 21–23. There has been also very interesting development within the framework of density functional theory to treat the movement of the electrons and the nuclei fully quantum mechanically.[24] However, all the explicitly time-dependent methods mentioned above should not be confused with TD-DFT (or TD-HF) quantum chemistry calculations for the determination of excited states (see, for example, Ref. 25).

This paper is organized as follows. In Sec. II we will briefly outline the theoretical methods we use to control the ultrafast molecular excitation, i.e., the TD-CIS method in Sec. II A and the basic aspects of the OCT in Sec. II B. In Sec. III the results for the short pulse excitation of *N*-methyl-6-quinolone molecule are presented. First, in Sec. III B some results from time-independent electronic structure calculations and a classical estimate for the time scale of the nuclear rearrangement after a vertical excitation are given. In Sec. III C we compare the performance of an ultrafast (two-level) π pulse to optimal field excitations and explore the effects of the multistate nature of our model. In Sec. IV we give a summary and an outlook to future work. We use a.u. throughout, if not stated otherwise.

II. THEORY

A. TD-CIS method

In the following we will briefly outline the TD-CIS method, which is described in more detail in Ref. 12. The underlying CIS (Ref. 26) calculation for a closed-shell molecule starts from the restricted Hartree-Fock (RHF) ground state Slater determinant,

$$|\Psi_0^{\mathrm{HF}}\rangle = \frac{1}{\sqrt{N!}}|(\psi_1\alpha),(\psi_1\beta),\ldots,(\psi_{N/2}\alpha),(\psi_{N/2}\beta)\rangle, \tag{1}$$

which is computed by solving the RHF equations,

$$\left[-\frac{1}{2}\boldsymbol{\nabla}^2 + \hat{v}_{\mathrm{ext}}(\mathbf{r}) + \hat{v}(\mathbf{r}) + \hat{v}_x\right]\psi_n = \varepsilon_n\psi_n. \tag{2}$$

Here, $\hat{v}_{\mathrm{ext}}(\mathbf{r})$ is the nuclear-electron attraction. The Coulomb potential, $\hat{v}(\mathbf{r})$, and the Hartree-Fock exchange, $\hat{v}_x$, are both due to the electron-electron interaction. For a molecule with N electrons the first $N/2$ solutions are occupied molecular orbitals, all others are unoccupied. Within the CIS approach additional Slater determinants are created by exciting an α electron from an occupied molecular orbital (MO) a to an unoccupied MO $r(\Psi_a^r)$, or by exciting a β electron $(\Psi_{\bar{a}}^{\bar{r}})$, respectively. Two such determinants can be combined to form a pure singlet state, a so-called singlet configuration state function (CSF),[27] which we will use in the following:

$${}^1\Psi_a^r = \frac{1}{\sqrt{2}}(\Psi_a^r + \Psi_{\bar{a}}^{\bar{r}}). \tag{3}$$

The field-free electronic Hamiltonian for a molecule with N electrons and N_A nuclei with charge Z_k,

$$\hat{H}_0 = -\frac{1}{2}\sum_{i=1}^{N}\boldsymbol{\nabla}_i^2 + \sum_{i=1}^{N}\sum_{j<i}^{N}\frac{1}{r_{ij}} - \sum_{k=1}^{N_A}\sum_{i=1}^{N}\frac{Z_k}{r_{ki}}, \tag{4}$$

is then used to calculate CI matrix elements within the basis of the RHF ground state Slater determinant and the singlet CSFs. By solving the eigenvalue equation for the corresponding CI matrix,

$$\mathbf{H}^{\mathrm{CIS}}\mathbf{D}_i = E_i^{\mathrm{CIS}}\mathbf{D}_i, \tag{5}$$

one gets excited state energies E_i^{CIS} and the excited state wave functions,

$$\Psi_i = D_{0,i}\Psi_0^{\mathrm{HF}} + \sum_{a=L}^{N/2}\sum_{r=N/2+1}^{M} D_{a,i}^r\,{}^1\Psi_a^r. \tag{6}$$

Here, L denotes the lowest occupied MO and M the highest unoccupied MO included in the CIS expansion. Note that the ground state energy and wave function are still given by the RHF solution for the CIS method.

We apply the time-dependent Schrödinger equation,

$$i\frac{\partial\Psi(t)}{\partial t} = \hat{H}(t)\Psi(t), \tag{7}$$

to describe the laser driven electron dynamics in our simulations. Here, $H(t)$ is a time-dependent electronic Hamiltonian,

$$\hat{H}(t) = \hat{H}_0 - \hat{\boldsymbol{\mu}}\mathbf{F}(t), \tag{8}$$

which consists of the field-free time-independent electronic Hamiltonian (4) and the interaction with the laser field $\mathbf{F}(t)$, treated by the semiclassical dipole approximation, with $\hat{\boldsymbol{\mu}} = -\Sigma_i^N\mathbf{r}_i + \Sigma_k^{N_A}Z_k\,\mathbf{R}_k$ being the molecular dipole operator. For the laser fields we use either fields computed by OCT (see Sec. II B) or $\cos^2$-shaped laser pulses,

$$\mathbf{F}(t) = \mathbf{f}(t)\cos[\omega(t-t_p)+\Phi], \tag{9}$$

$$\mathbf{f}(t) = \begin{cases}\mathbf{f}_0\cos^2[\pi/(2\sigma)(t-t_p)] & \text{if } |t-t_p|<\sigma\\ \mathbf{0} & \text{else.}\end{cases} \tag{10}$$

$\mathbf{f}_0$ gives the maximal amplitude of the laser pulse envelope which is reached at t_p. The frequency, full width at half maximum (FWHM), and the phase of the laser pulse are determined by ω, σ, and Φ.

We use the CIS states to expand the time-dependent electronic wave function as

$$\Psi(t) = \sum_i C_i(t)\Psi_i, \tag{11}$$

where the initial wave function at $t=0$ is the RHF ground state. For the time evolution of the coefficient vector $\mathbf{C}(t)$ we apply an operator splitting technique,[28]

$$\mathbf{C}(t+\Delta t)=\left[\prod_{j=x,y,z}\mathbf{U}_j^{\dagger}e^{-iF_j(t)\tilde{\boldsymbol{\mu}}_j\Delta t}\mathbf{U}_j\right]e^{-i\tilde{\mathbf{H}}\Delta t}\mathbf{C}(t). \quad (12)$$

Here, $\tilde{\mathbf{H}}$ is the diagonal Hamilton matrix in CIS eigenstate basis. $\mathbf{U}_j$ $(j=x,y,z)$ are unitary matrices which transform from the CIS eigenstate basis to a basis in which the dipole matrices $\tilde{\boldsymbol{\mu}}_j$ are diagonal.

B. Optimal control theory

Within the framework of OCT,[9,10] it is possible to compute perfectly suited laser fields in order to drive the quantum dynamical system to some specified target state. Here, we adopt an iterative algorithm introduced by Rabitz *et al.*[29,30] and only want to give a short recapitulation of the method.

The starting point is a positive definite target operator, $\hat{O}$, for which the expectation value should be maximal at the control time t_f, i.e., the final time of the propagation. With this operator the following constrained objective functional can be constructed:

$$J=\langle\Psi(t_f)|\hat{O}|\Psi(t_f)\rangle-\int_0^{t_f}\alpha(t)|\mathbf{F}(t)|^2dt - 2\,\mathrm{Re}\left[\int_0^{t_f}\langle\chi(t)|\frac{\partial}{\partial t}+i(\hat{H}_0-\hat{\boldsymbol{\mu}}\mathbf{F}(t))|\Psi(t)\rangle dt\right]. \quad (13)$$

Here, $\alpha(t)$ is a positive function, which can be used to control the energy contained in the optimal field. We use a time-dependent value of α computed as

$$\alpha(t)=\alpha/s(t),\quad s(t)=\exp(-[(t-t_m)/\Delta t_s]^{N_s}), \quad (14)$$

in order to have some influence on the shape of the optimal laser field. The values of t_m, Δt_s, and N_s are given in Sec. III C. $\chi(t)$ is a Lagrange multiplier introduced by the constraint, that the time evolution of the system should be given by the time-dependent Schrödinger equation. Computing the stationary points of the objective functional, i.e., $\delta J=0$, results in three coupled equations for the wave function, the Lagrange multiplier $\chi(t)$, and the optimized field,

$$i\dot{\Psi}(t)=(\hat{H}_0-\hat{\boldsymbol{\mu}}\mathbf{F}(t))\Psi(t)\quad\text{with }\Psi(t_0)=\Psi_0, \quad (15)$$

$$i\dot{\chi}(t)=(\hat{H}_0-\hat{\boldsymbol{\mu}}\mathbf{F}(t))\chi(t)\quad\text{with }\chi(t_f)=\hat{O}\Psi(t_f), \quad (16)$$

$$\mathbf{F}(t)=-\frac{1}{\alpha(t)}\,\mathrm{Im}[\langle\chi(t)|\hat{\boldsymbol{\mu}}|\Psi(t)\rangle]. \quad (17)$$

Equations (15) and (16) are time-dependent Schrödinger equations, which can be solved as described in Sec. II A. However, they are coupled through Eq. (17) and have different boundary conditions. Therefore, it is not straightforward to obtain a solution for the optimal field, $\mathbf{F}(t)$. We use the iterative procedure given in Ref. 30, where one starts with an initial trial field and gets after several back and forward propagations a converged field which corresponds to a local optimal solution.

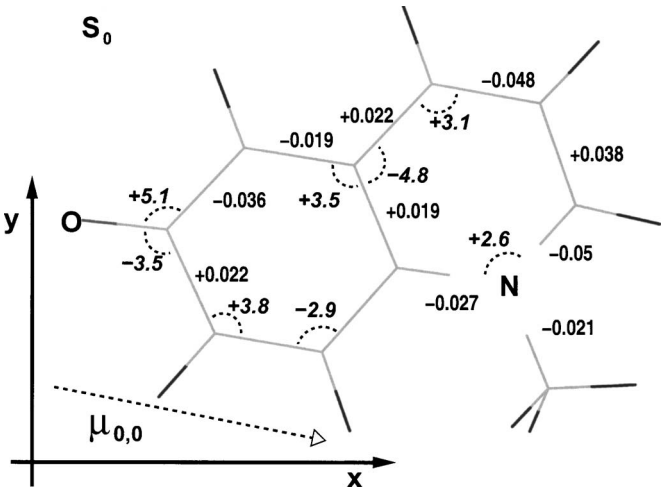

FIG. 1. Shown is the optimized geometry for the RHF ground state (S_0) computed with the 6-31G* basis set together with the main structural differences in the optimized CIS S_1 state. Bond length differences larger than 0.01 Å (nonitalic numbers) and bond angle changes larger than 2.5° (italic numbers) are given. Also indicated is the orientation of the coordinate system used and the orientation of the ground state permanent dipole, which differs only very slightly from the one for the S_1 state. The origin of the coordinate system is always set to the center of mass of the molecule.

III. RESULTS

A. Stationary RHF and CIS calculations

The stationary quantum chemical calculations are performed using the GAUSSIAN 03 program package,[31] with a 6-31G* (Ref. 32) basis set. We use RHF for the ground state calculations and CIS (Ref. 26) for the excited states. The optimized structure of the S_0 state together with the main structural differences in the optimized S_1 state are shown in Fig. 1. The planar molecule has a ground state dipole moment of $4.66ea_0$ (11.8 Debye), which is roughly oriented along the N–O axis. The transition dipole moment for the $S_0\rightarrow S_1$ transition lies also in the molecular plane. Quantitatively, we find $\boldsymbol{\mu}_{0,0}=(4.575,-0.886,0)\ ea_0$ for the permanent S_0 dipole moment (as indicated in Fig. 1), and $\boldsymbol{\mu}_{0,1}=(-1.143,-1.160,0)\ ea_0$ for the $S_0\rightarrow S_1$ transition dipole moment using the coordinate system shown in Fig. 1. For the first excited state S_1 we obtain a vertical excitation energy of 0.1148 E_h (3.12 eV, 397 nm). In the vertically excited molecule the dipole moment drops to $2.89ea_0$ (7.35 D) according to the CI density method.[33] If the dipole moment is calculated directly from the CIS wave function, one finds $|\boldsymbol{\mu}_{1,1}|=1.79ea_0$. Hence, the dipole moment decreases significantly upon electronic excitation.

Looking at the main structural differences in the S_1 geometry in Fig. 1, one can see that the overall change in the molecular structure is very small. Altogether the molecule undergoes a slight rearrangement of the heavy atoms in the molecular plane. However, we get an excitation energy for the vertical transition from the electronic ground state to the S_1 state at the optimized excited state geometry of 0.0906 E_h (2.47 eV, 503 nm), which corresponds to a notable intramolecular Stokes shift of roughly 0.024 E_h (0.65 eV). Also, the dipole moment of the excited state is further reduced to $2.74ea_0$ (6.96 D) when computed, with the CI density method, at the optimized S_1 geometry.

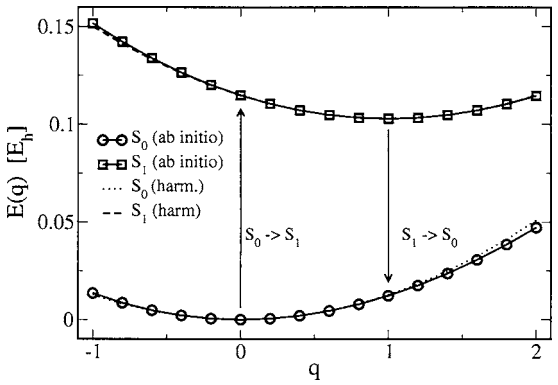

FIG. 2. Shown are the RHF/CIS potential energy curves along the linear transit coordinate from the optimized S_0 geometry, at $q=0$, to the one of the S_1 state, at $q=1$ (solid lines). Also displayed are the harmonic approximations for both potential curves (dashed and dotted).

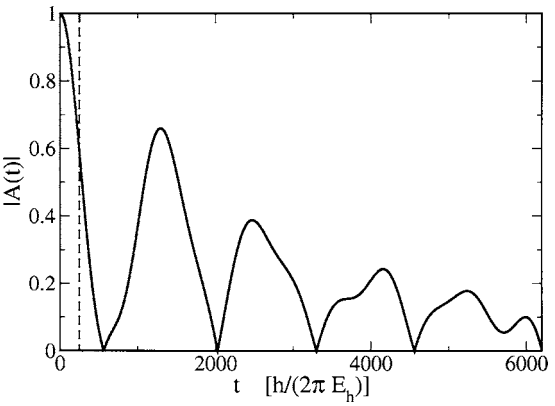

FIG. 3. Shown is the absolute value of $A(t)$ for the nuclear dynamics on the harmonic S_1 potential after vertical excitation from the S_0 equilibrium geometry. The vertical dashed line indicates a time of 250 $\hbar/E_h$ after which we want to achieve an ultrafast excitation (see Sec. III C).

These results are in reasonable agreement with experimental data recorded in water,[11] where the stationary absorption band is observed at ≈410 nm, corresponding to a vertical transition. The time-dependent stimulated emission from the excited state sets in at 515 nm and reaches a value of 612 nm for longer times. The second excited state S_2 is clearly separated in energy from the S_1 state, and has a vertical excitation energy from the S_0 state of 0.174 E_h (4.72 eV) for the optimized S_0 geometry and 0.168 E_h (4.57 eV) for the optimized S_1 geometry.

B. Time scale of the intramolecular Stokes shift

We also computed a linear transit path from the optimized S_0 geometry to the optimized S_1 geometry in order to explore the nature of the ground and excited state potential energy surfaces (PES) in more detail. We also wish to estimate the time scale on which nuclear motion sets in. This time scale sets the clock for the laser pulses to be used to induce purely electronic dynamics below. Let $\mathbf{Q}_{S_0}$ and $\mathbf{Q}_{S_1}$ be the vectors containing the mass weighted Cartesian coordinates of all atoms of the optimized structures. We then define our linear transit coordinate as

$$\mathbf{Q}_{lt} = \mathbf{Q}_{S_1} - \mathbf{Q}_{S_0}. \tag{18}$$

The CIS energies are calculated along this path depending on a dimensionless parameter q, where $q=0$ corresponds to the optimal geometry for the S_0 state, and $q=1$ to that for the S_1 state,

$$E_j(q) = E_j^{\mathrm{CIS}}(\mathbf{Q}_{S_0} + q\mathbf{Q}_{lt}). \tag{19}$$

Here, j indicates the electronic state, i.e., $j=0$ for the S_0 state, the HF ground state, and $j=1$ for the first excited state, S_1. Figure 2 shows the computed potential energy curves together with a harmonic fit along the linear transit coordinate. For this fit the linear transit coordinate expressed in mass weighted Cartesian displacement coordinates is projected on the normal modes $\mathbf{Q}_{j,i}$ obtained from a frequency analysis performed at the corresponding equilibrium geometry of the jth state,

$$\tilde{\mathbf{Q}}_{lt} = \sum_i \mathbf{Q}_{j,i}\mathbf{Q}_{j,i}^{\dagger}\mathbf{Q}_{lt} = \sum_i c_{j,i}\mathbf{Q}_{j,i}. \tag{20}$$

The approximated harmonic energy $E_j^{\mathrm{harm}}(q)$ is easily obtained from the $c_{j,i}$ as

$$E_j^{\mathrm{harm}}(q) = \frac{1}{2}\sum_i \omega_{j,i}^2 (c_{j,i}q)^2, \tag{21}$$

where $\omega_{j,i}$ is the frequency of normal mode i in state j.

As displayed in Fig. 2, the harmonic approximation is quite accurate for the low amplitude motion considered here. In order to estimate the time scale of the nuclear rearrangement dynamics after a vertical $S_0 \rightarrow S_1$ transition, we compute the time-dependent position autocorrelation function, $A(t)$, assuming purely classical harmonic oscillators for the vibrational motion,

$$A(t) = \frac{1}{W}\sum_i c_{j,i}^2 \cos(\omega_{j,i}t), \tag{22}$$

with $j=1$, and W is an appropriate normalization factor,

$$W = \sum_i c_{j,i}^2. \tag{23}$$

In Fig. 3 the absolute value of $A(t)$ is shown. As one can see $|A(t)|$ shows an oscillatory behavior, and drops to zero for the first time in about 500 $\hbar/E_h$ or 12 fs. From Fig. 3 we estimate that in order to enforce a vertical transition, a laser pulse not longer than about 250 $\hbar/E_h$ or 6 fs should be used. After this time, nuclear motion is expected to set in, and the frozen-nuclei approximation becomes questionable. In the next section, we will attempt to enforce a state-selective excitation $S_0 \rightarrow S_1$ with short (i.e., energetically broad and intense) laser pulses, despite in our model a multitude of other excited states is present. The time scale of 6 fs for the onset of nuclear rearrangement seems to be very long in the presence of high frequency vibrations as C–H stretches in the molecule. For example, a transition frequency of 3000 cm^{-1} corresponds to a vibrational period of ≈11 fs. However, the optimized C–H bond lengths show only very small differences between the optimized S_0 and S_1 structures. The maximal change is 0.005 Å and on average the bond lengths

change by 0.002 Å. Therefore, the high frequency vibration modes are only displaced very slightly upon excitation and, thus, nearly no nuclear dynamics is induced in these modes.

C. Ultrafast electronic excitations

In this section we simulate the laser induced excitation of *N*-methyl-6-quinolone by means of the TD-CIS method within the fixed nuclei approximation. As shown in the last section, this approximation should be reasonable at least for propagation times in the order of 250 $\hbar/E_h$ (≈6 fs). However, in order to explore the different excitation pathways for different time scales, we will also investigate the laser driven electron dynamics for longer pulse durations. For the dynamical simulations we use again the 6-31G* basis set and all unoccupied and all occupied MOs, except the ones corresponding to the 1*s* atomic orbitals of the heavy atoms (C,O,N) to form the CSFs. This gives in total 4681 singlet CSFs including the HF ground state. In our dynamical calculations we used one- and two-electron integrals in atomic orbital basis computed by the quantum chemistry program package GAMESS.[34] All other quantities described above were recalculated as an internal consistency check prior to the propagations.

The laser fields were optimized fields from the OCT calculations. For comparison, resonant $\cos^2$-shaped π pulses[28] are also used. A π pulse induces a total inversion population in an ideal two-level system and it can be constructed within the rotating wave approximation[35] from the condition $|\mathbf{f}_0|\sigma = \hbar\pi/|\boldsymbol{\mu}_{0,1}|$, when the field amplitude $\mathbf{f}_0$ and the transition dipole $\boldsymbol{\mu}_{0,1}$ are parallel.

For all propagations we use a time step $\Delta t = 0.1\ \hbar/E_h$ (2.4 as), which gave converged results for the most intense π pulse considered below. We applied π pulses with total pulse durations (2×FWHM) of 250, 500, 1000, 2000, and 4000 $\hbar/E_h$ and performed OCT calculations for control times t_f of 250, 500, and 1000 $\hbar/E_h$. Our target operator is the projector on the S_1 state, i.e., $\hat{O} = |\Psi_1\rangle\langle\Psi_1|$.

To allow for more flexibility in the optimal field we used a shaped penalty function $\alpha(t)$ as given in Eq. (14). Here, we took $N_s = 12$, $t_m = t_f/2$, and Δt_s as 220, 440, and 830 $\hbar/E_h$. For α we take 10, 20, and 40 $e^2a_0^2/E_h$ in order to get about the same pulse energy as in the π-pulse case, and hence make both pulses comparable. With this choice we get a maximal increase of 30% in the energy of the OCT pulse relative to the π pulse. We tried different initial fields, both random fields and π pulses, for the iterative optimal control algorithm. It turned out that in our multistate model many locally optimal fields exist, depending on the trial field (see discussion below). However, as in our test calculations the efficiency of these different fields was nearly the same, we used for all results below a $\cos^2$-shaped π pulse as the initial field. We also assume our laser pulse to propagate along *z*, i.e., we set the *z* component of the laser field to zero for all times. To achieve reasonably converged optimal fields 30 iterations were needed.

The final populations in the S_1 state for the π-pulse fields and the optimal fields as a function of the total pulse duration and the control time are given in Fig. 4. As already shown in

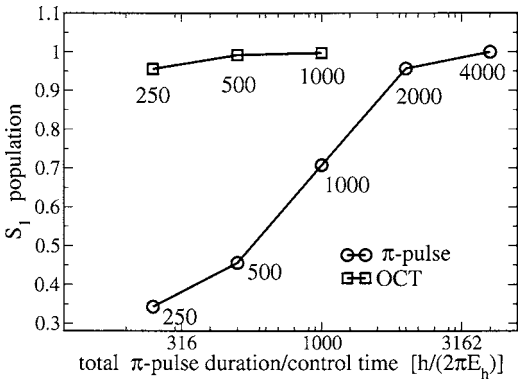

FIG. 4. Shown are the final S_1 populations for a series of π pulses (circles) as a function of the total pulse duration (2×FWHM) and the same for OCT fields (squares) as a function of the control time (details see text).

Ref. 8, for short pulse lengths the π pulses become very unselective because of multiphoton transitions and other effects induced by the polarizability and higher order polarizabilities. In the present case the final population in the S_1 state drops from over 99.9% for a total pulse duration of 4000 $\hbar/E_h$ (97 fs) to 34.2% for 250 $\hbar/E_h$ (6 fs). In contrast, the laser fields obtained from the OCT are highly selective, even for very short final times. For a control time of 250 $\hbar/E_h$, we still achieve a final population in the target state of 95.5%. This means that by applying the OCT we can achieve a selective excitation from the S_0 to the S_1 state in about 250 $\hbar/E_h$, which should be rather close to the ideal picture of a vertical transition considering the findings in Sec. III B. For even longer control times the OCT field is rapidly approaching to the optimal value of 100%, reaching already 99.7% population for a control time of 1000 $\hbar/E_h$ (24 fs). In contrast, the corresponding π pulse gives a yield of only 70.7%.

The laser fields for the propagations with a pulse duration or control time of 250 $\hbar/E_h$ (6 fs) are given in Fig. 5. Figure 5(a) shows the field component parallel to the dipole transition moment of the $S_0 \rightarrow S_1$ transition for the π pulse,

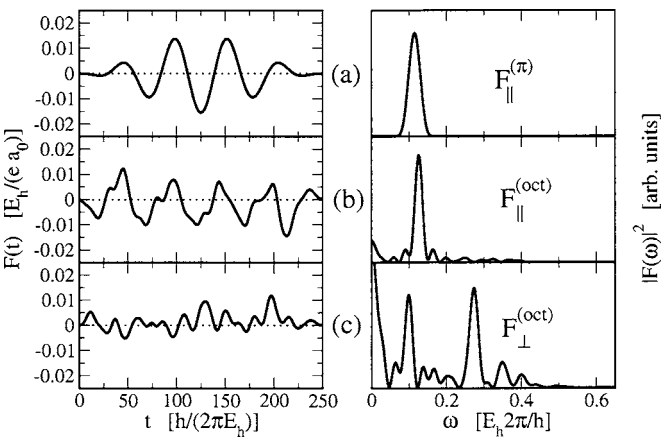

FIG. 5. Shown are the field components parallel to the dipole transition moment of the $S_0 \rightarrow S_1$ transition, $F_\parallel$, for the π pulse (a) and for the OCT field (b). For the OCT field also the component perpendicular to the dipole transition moment, $F_\perp$, is shown (c). On the left the time-dependent field components are displayed, on the right the corresponding frequency distributions.

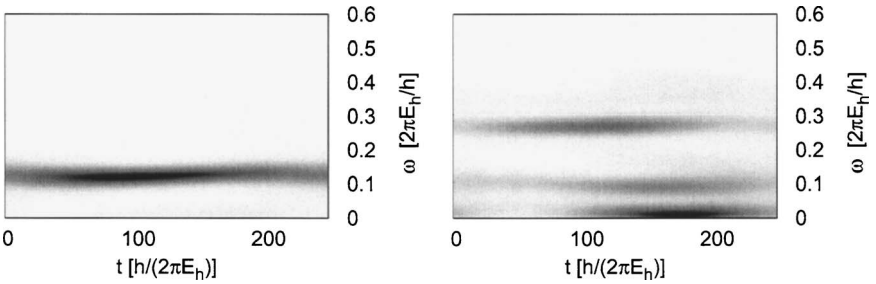

FIG. 6. Shown are the Husimi distributions of the OCT field for the field component parallel to the dipole transition moment of the $S_0 \rightarrow S_1$ transition (left graph) and for the perpendicular one (right graph). The dark areas indicate a high value of the distribution function.

$F_{\parallel}^{(\pi)}$; (b) the parallel component for the OCT field, $F_{\parallel}^{(\mathrm{oct})}$. For the OCT field, there is also a component $F_{\perp}^{(\mathrm{oct})}$ perpendicular to the dipole transition moment which is displayed in Fig. 5(c). On the left of Fig. 5 the time-dependent fields are displayed, and on the right the corresponding frequency distributions. If one first compares the parallel fields in (a) and (b), one can see that they are quite similar. There is a main peak for both the OCT field and the π pulse around the resonance frequency of 0.1148 E_h. Not only the peak position but also the maximal absolute field strengths are comparable, i.e., 0.0154 $E_\mathrm{h}/(ea_0)$ $(7.9\times10^9$ V/m) for the π pulse and 0.0145 $E_\mathrm{h}/(ea_0)$ $(7.5\times10^9$ V/m) for the OCT field. Note that the total pulse energy is only $\approx$9% higher for the OCT field, than for the π-pulse.

The origin and purpose of the perpendicular component of the OCT field are much harder to understand. In Fig. 5(c) one can see three main frequency components. There is one static, dc-like component, at nearly zero frequency, and two others around 0.1 and 0.28 $E_\mathrm{h}/\hbar$. However, there is no easy explanation of these frequencies in terms of transition energies or transition dipole moments, obtained from the field-free, stationary quantum chemistry calculations. We also performed a propagation using only the parallel field component of the OCT field, neglecting the perpendicular one. Such a propagation yields only 74.7% final population in the target state, which is a strong indication that the perpendicular component is important. Also, only 13.3% of the final population is still in the ground state, which means that 12% of the population is excited to higher states. As the main frequency component of the parallel field is mainly centered around the resonance frequency for the $S_0 \rightarrow S_1$ transition, it seems reasonable to assume that this amount of excitation can be attributed to multiphoton transitions.

For a further analysis of the OCT field we calculated the Husimi distribution,[36] $Q(t,\omega)$, of the two field components,

$$Q(t,\omega) = \int\int W(t',\omega')\exp[-(t-t')^2/(2\sigma_t^2) - (\omega-\omega')^2/(2\sigma_\omega^2)]dt'd\omega', \quad (24)$$

which is the Wigner[37] distribution, $W(t,\omega)$, convoluted with a minimum uncertainty Gaussian in ω and t (for a comprehensive review see, for example, Ref. 38),

$$W(t,\omega) = \frac{1}{\pi}\int F^{\star}(t-t')F(t+t')\exp(-2i\omega t')dt'. \quad (25)$$

From the Husimi distribution one can conveniently deduce simultaneous information about the laser pulse in frequency and time domain.

The Husimi distribution of the parallel OCT field component is shown in the left graph of Fig. 6, the one for the perpendicular component in the right graph. Both distributions are calculated with a width parameter $\sigma_t=50\ \hbar/E_\mathrm{h}$ in Eq. (24), which implies $\sigma_\omega=0.02\ E_\mathrm{h}/\hbar$. One can see that the two low frequency components of the perpendicular field are maximal at later times compared to the temporal distribution of the parallel component. We believe that the rather strong field of the laser pulse induces a dynamic polarization in the molecule, already after short times. The later part of our optimal field is then strongly influenced by this polarization and the OCT adapts to the current state of the molecule. This interpretation is also supported by the fact that the actual shape of the optimal fields strongly depends on the initial trial field. In the present example, even a change in the sign of an initial π-pulse field results in a quite different optimal field, where, for example, the frequency component at 0.1 $E_\mathrm{h}/\hbar$ is completely missing. This means that the initial field direction, or in other words the early polarization of the molecule, determines the optimal field at later propagation times. The polarization of the molecule is, in the TD-CIS model, mainly due to the presence of a multitude of higher excited states. A two-state model comprising of states S_0 and S_1 alone, therefore, cannot account for this effect.

In order to get a quantitative estimate of how much our results are influenced by polarization effects, we performed calculations including only a certain subset of excited states. As the polarizability and higher order polarizabilities are caused by the multistate nature of our theoretical model, their influence should become smaller; the fewer excited states are included in our propagations.

We performed calculations for a total pulse duration and control time of 250 $\hbar/E_\mathrm{h}$, including only the first 2, 20, 200, and 2000 lowest lying electronic states, respectively. The final population in the S_1 state as a function of the number of states is shown in Fig. 7, both for π pulse and for optimal field excitation. Interestingly, the π pulse induces a nearly perfect population inversion (to over 99%), if we only include the S_0 and S_1 states in the propagation. This means that even for such a few cycle pulse the rotating wave approximation is reasonable. Including $\geqslant$20 states leads to a dramatic loss of efficiency of the π pulse, because higher states are populated in expense of S_1. In contrast, the OCT field keeps the population of the target state high. Including 20 or 200 states in the propagation already accounts for the major part of the multistate effects in the calculations for the π pulses and the OCT fields. However, only the propagations with 2000 states yield the same population and nearly the same optimal field as the full propagations with 4681 states.

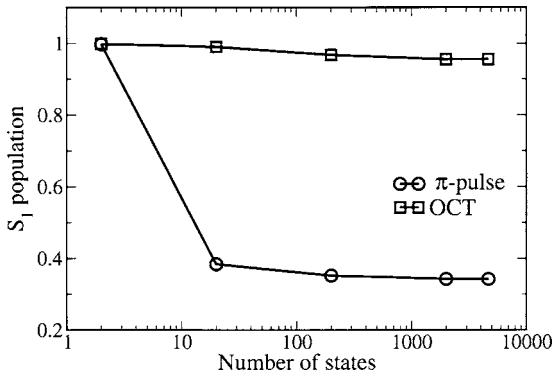

FIG. 7. Shown are the final S_1 populations for a π pulse (circles) as a function of the number of states included in the propagations and the same for OCT fields (squares). All results are for a total π-pulse duration and control time of 250 $\hbar/E_h$.

This clearly shows that few-state models are questionable when ultrashort, intense laser sources are used.

One could argue that, if such high lying states are needed to successfully simulate the laser driven dynamics for the fields under consideration, this will lead to complete ionization of the molecule rather than to a state to state transition. Indeed, the ionization channel is totally neglected in our calculations, because we use atom centered contracted Gaussian type orbitals as basis functions. In order to get a crude estimate on the importance of ionization in the real molecule, we applied the following procedure. From Koopmans' theorem we find an approximate ionization potential of 0.230 54 E_h. For a control time as short as 250 $\hbar/E_h$, which is the shortest pulse in our OCT calculations, we calculated the time-dependent probability, $P^{(nb)}(t)$, for the molecule to be in any excited state with an excitation energy larger than that threshold. The maximum value of $P^{(nb)}(t)$ we get in this way is about 15%. We believe that this is a reasonable first order approximation for the amount of ionization induced by the computed optimal field, and, therefore, that ionization is quantitatively important but not dominant in a realistic application. Further, one may also criticize the quality of the CIS excited states. Here we state that again, the polarization effects and hence the OCT field will quantitatively depend on the accuracy of the excited state, but all qualitative statements made in this paper will survive. Apart from this, the TD-CI method is systematically improvable by taking higher excitations either perturbatively or exactly into account. Another difficulty for a realistic application of the results is that they depend critically on the orientation of the molecule in all three axes. It has been shown by Larsen *et al.*[39] that such an orientation can be achieved by elliptically polarized laser fields in a molecular beam experiment. However, it might be harder or even impossible to achieve such an orientation in condensed phase. Even so, the conclusions drawn about the importance of multistate models for the description of ultrafast laser excitation would still apply for randomly oriented molecules.

IV. CONCLUSIONS AND OUTLOOK

We computed optimal laser fields for an ultrafast (≈6 fs) excitation of a polyatomic molecule, *N*-methyl-6-quinolone. This was achieved by combining the recently introduced multistate TD-CIS method with OCT. It has also been shown that the ultrafast excitation is strongly influenced by multiphoton transitions and other effects of the polarizability or even higher order polarizabilities. The exact findings of our calculations are only qualitatively in the sense that a one to one experimental realization of such an excitation might be very hard to achieve, because of the assumed orientation of the molecule, the time-dependent laser fields needed, and the quality of the underlying electronic structure model. However, qualitatively our results will still be important. For future work we plan to perform a systematic investigation how much these nonlinear effects depend on the quality of the underlying electronic structure method, e.g., the basis set and/or the length of the CI expansion.

ACKNOWLEDGMENTS

We thank P. Saalfrank, N. Ernsting, and Y. Ohtsuki for fruitful discussions and gratefully acknowledge support of this work by the Deutsche Forschungsgemeinschaft through the SFB 450 (subproject C7).

[1] A. H. Zewail, J. Phys. Chem. A **104**, 5660 (2000).
[2] J. Manz, in *Femtochemistry and Femtobiology*, edited by V. Sundström (Imperial College Press, London, 1996), Vol. 101, pp. 80–318.
[3] M. Drescher, M. Hentschel, R. Kienberger, M. Uiberacker, V. Yakovlev, A. Scrinzi, T. Westerwalbesloh, U. Kleineberg, U. Heinzmann, and F. Krausz, Nature (London) **419**, 803 (2002).
[4] A. Föhlisch, P. Feulner, F. Hennies, A. Fink, D. Menzel, D. Sanchez-Portal, P. M. Echenique, and W. Wurth, Nature (London) **436**, 373 (2005).
[5] J. Breidbach and L. S. Cederbaum, J. Chem. Phys. **118**, 3983 (2003).
[6] G. G. Paulus, F. Lindner, H. Walther, A. Baltuška, E. Goulielmakis, M. Lezius, and F. Krausz, Phys. Rev. Lett. **91**, 253004 (2003).
[7] X. Liu, H. Rottke, E. Eremina *et al.*, Phys. Rev. Lett. **93**, 263001 (2004).
[8] P. Krause, T. Klamroth, and P. Saalfrank, J. Chem. Phys. **123**, 074105 (2005).
[9] S. Shi, A. Woody, and H. Rabitz, J. Chem. Phys. **88**, 6870 (1988).
[10] R. Kosloff, S. A. Rice, P. Gaspard, S. Tersigni, and D. J. Tannor, Chem. Phys. **139**, 201 (1989).
[11] J. L. P. Lustres, S. A. Kovalenko, M. Mosquera, T. Senyushkina, W. Flasche, and N. P. Ernsting, Angew. Chem., Int. Ed. **44**, 5635 (2005).
[12] T. Klamroth, Phys. Rev. B **68**, 245421 (2003).
[13] K. Harumiya, I. Kawata, H. Kono, and Y. Fujimura, J. Chem. Phys. **113**, 8953 (2000).
[14] J. Colgan, S. D. Loch, M. S. Pindzola, C. P. Ballance, and D. C. Griffin, Phys. Rev. A **68**, 032712 (2003).
[15] K. C. Kulander, Phys. Rev. A **36**, 2726 (1987).
[16] E. Runge and E. K. U. Gross, Phys. Rev. Lett. **52**, 997 (1984).
[17] D. Hegarty and M. A. Robb, Mol. Phys. **38**, 1795 (1979).
[18] J. Zanghellini, M. Kitzler, C. Fabian, T. Brabec, and A. Scrinzi, Laser Phys. **13**, 1064 (2003).
[19] T. Kato and H. Kono, Chem. Phys. Lett. **392**, 533 (2004).
[20] M. Nest, T. Klamroth, and P. Saalfrank, J. Chem. Phys. **122**, 124102 (2005).
[21] M. Ben-Nun, J. Quenneville, and T. J. Martínez, J. Phys. Chem. A **104**, 5161 (2000).
[22] P. A. Hunt and M. A. Robb, J. Am. Chem. Soc. **127**, 5720 (2005).
[23] M. Hartmann, J. Pittner, and V. Bonačić-Koutecký, J. Chem. Phys. **114**, 2123 (2001).
[24] T. Kreibich and E. K. U. Gross, Phys. Rev. Lett. **86**, 2984 (2001).

[25] R. Bauernschmitt and R. Ahlrichs, Chem. Phys. Lett. **256**, 454 (1996).
[26] J. B. Foresman, M. Head-Gordon, J. A. Pople, and M. J. Frisch, J. Phys. Chem. **96**, 135 (1992).
[27] R. Paunz, *Spin Eigenfunctions* (Plenum, New York, 1979).
[28] A. D. Bandrauk, E. Aubanel, and S. Chelkowski, in *Femtosecond Chemistry*, edited by J. Manz and L. Wöste (Verlag Chemie, Weinheim, 1995), Vol. 2, Chap. 25, p. 731.
[29] W. Zhu, J. Botina, and H. Rabitz, J. Chem. Phys. **108**, 1953 (1998).
[30] W. Zhu and H. Rabitz, J. Chem. Phys. **109**, 385 (1998).
[31] M. J. Frisch, G. W. Trucks, H. B. Schlegel *et al.*, Gaussian 03, revision c.02, Gaussian, Inc., Wallingford, CT, 2004.
[32] P. C. Hariharan and J. A. Pople, Theor. Chim. Acta **28**, 213 (1973).
[33] K. B. Wiberg, C. M. Hadad, T. J. LePage, C. M. Breneman, and M. J. Frisch, J. Phys. Chem. **96**, 671 (1992).
[34] M. W. Schmidt, K. K. Baldridge, J. A. Boatz *et al.*, J. Comput. Chem. **13**, 1347 (1993).
[35] I. I. Rabi, Phys. Rev. **51**, 652 (1937).
[36] K. Husimi, Proc. Phys. Math. Soc. Jpn. **22**, 264 (1940).
[37] E. Wigner, Phys. Rev. **40**, 749 (1932).
[38] H.-W. Lee, Phys. Rep. **259**, 147 (1995).
[39] J. J. Larsen, K. Hald, N. Bjerre, H. Stapelfeldt, and T. Seideman, Phys. Rev. Lett. **85**, 2470 (2000).